

# A Novel Torsional Actuator Augmenting Twisting Skeleton and Artificial Muscle for Robots in Extreme Environments

Zhujin Jiang and Ketao Zhang\*

**Abstract**—Torsional actuators are a class of artificial muscle technology that generates torque and produces rotary motion in response to various stimuli. This paper presents a novel torsional actuator combining an origami-inspired twisting skeleton and an artificial muscle. The process of torsional actuator design starts from identifying a foldable twisting skeleton which is capable of achieving helical motion thereby translating linear motion to rotational motion. This is followed by the integration of an artificial muscle to drive the twisting skeleton. Kinematics of both the twisting skeleton and artificial muscle are analyzed. Following the design and kinematic analysis, a prototype is developed by bonding 3D printed polylactic acid (PLA) parts and thermoplastic polyurethane (TPU) films to form the twisting skeleton and laminating TPU membranes by using heat sealing tools to form the artificial muscle. A pneumatic control system is built to evaluate the performances of torsional actuator by testing the relationship between twisting angle, air pressure, driving force and output torque. Experimental results show that the relationship between air pressure, driving force and output torque is proportional at a given twisting angle. The novel torsional actuator augmenting an origami-inspired skeleton and soft artificial muscle leads to simplified analytical model and has potential of driving robotic systems in environment where pneumatically actuated systems are preferred over electrical machines and drives.

## I. INTRODUCTION

In recent years, rigid-bodied robots [1], [2], [3] have been extensively explored and developed to perform various tasks in challenging environments [4]. These robots are driven by electrical motors and able to quickly respond to control signals thereby rapidly adjusting their contacts with the ground to move stably and keep balance. However, working in some extreme environments such as high temperature, nuclear plants, combustible gas and oil is still a tough challenge for them as their actuators and batteries could be easily damaged by heat and radiation, or cause explosion of fuel. By contrast, soft legged robots like pipe-climbing robot [5] and modular quadruped robot [6] powered by pneumatic actuators are lightweight and can be fabricated by flexible materials such as heat resistant and fatigue resisting fabric, which allow them to be applied to extreme scenarios such as radiation. The soft robot with integrated fluidic circuit, switches and actuators [7] is also able to walk and grasp in combustible oil and gas environments. However, the deformations of most soft robots are continuous, complex and highly compliant

without well-understood kinematic models. These factors have negative influences on the motion control of soft robots [8]. Origami-folding structures are considered to bridge this gap between rigid-bodied robots and soft machines as they have the characteristics of deployability and portability [9], can be precisely modeled for dynamic control and also can be fabricated by foldable fatigue resisting materials.

Torsional actuators, also known as torsional artificial muscles, generate torque and produce rotary motion in response to various stimuli such as heating, electrochemical charging or chemical absorption [10]. Fluid is a practical way to actuate artificial muscles as it is safe to users and friendly to environment. For instance, two McKibben artificial muscles with inner tubes driven by pneumatic pressure serve as a biomimetic torsional actuator for human-like robot limbs [11], [12]. Antagonistic torsion shape actuators composed of two oppositely oriented helix like structures are pneumatically driven to achieve pure rotational motion with minimal linear motion [13]. Furthermore, the soft pneumatic torsional actuators developed in [5], [6] can achieve twisting-contraction motion when they are vacuumed. They are also able to perform multiple motions including linear, twisting and radial movements by connecting each other in different ways. These actuators above do not have skeleton, leading to limited stiffness.

Origami folding techniques are able to convert a 2D thin sheet into 3D objects by folding flexible creases [14] to increase stiffness and realize the required functions [15], which provides inspiration for scientists and engineers in finding feasible solutions for engineering problems in robotics field. For example, an origami twisted tower is applied to a robotic manipulator with three finger [16] and Kresling crease pattern nested inside a paper bellow is used for constructing a crawling robot [17]. Besides, a stiffening mechanism based on the origami principle of perpendicular folding is employed to increase the structural stiffness of an unmanned aerial vehicle with self-locking robotic arm [18]. A crawling robot which can autonomously fold itself from a flat sheet with embedded electronics to a functional machine is also developed [19]. Further, origami-inspired artificial muscles [20] can not only provide softness and achieve multi-axial controllable motions but also generate high stresses when vacuumed or inflated. A twisting mechanism using origami folding techniques allows helical motion and is employed to convert translational motion to rotation [21].

In this work, we propose a novel torsional actuator augmenting a twisting skeleton and an artificial muscle. A parallel foldable origami structure is employed as the twist-

\*This work was partially supported by research awards from the Engineering and Physical Sciences Research Council (EPSRC) projects, National Centre for Nuclear Robotics (NCNR) EP/R02572X/1, NCNR Flexifunds Grant and Queen Mary University of London Start-up fund, China Scholarship Council (CSC). (Ketao Zhang is corresponding author.)

Centre for Advanced Robotics (ARQ), Queen Mary University of London  
z.jiang@qmul.ac.uk, ketao.zhang@qmul.ac.uk

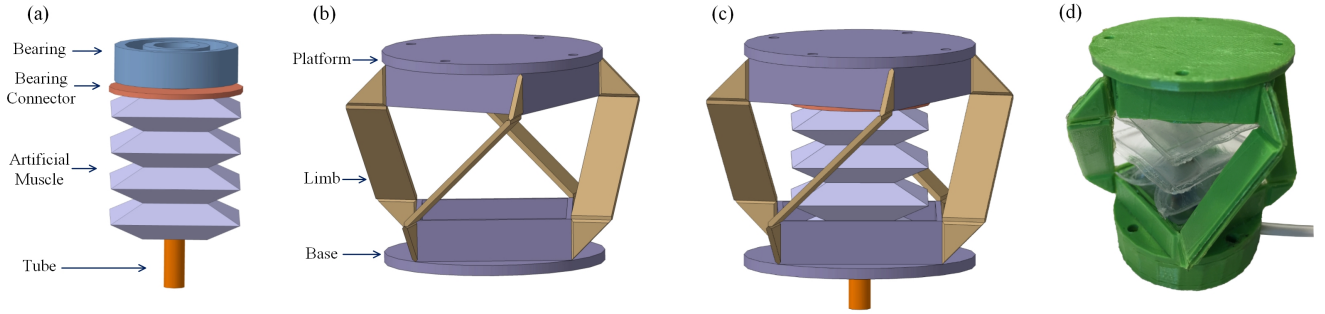


Fig. 1. Design of the torsional actuator. (a) internal structure of the torsional actuator, (b) twisting skeleton of the torsional actuator, (c) the whole structure of the torsional actuator, (d) prototype of the torsional actuator.

ing skeleton while a multilayer square artificial muscle is designed to drive the twisting skeleton. The twisting skeleton is fabricated by 3D printing polylactic acid (PLA) parts and bonding them with thermoplastic polyurethane (TPU) films. The artificial muscle is produced through laminating TPU membranes on heat press machine to form air pouches which are then connected with each other by heat sealer. The proposed torsional actuator is driven by air pressure and is durable in some extreme environments such as radiation where electrical actuators are sensitive and easily damaged. The contributions of this work include

- 1) The origami-folding inspired concept design and kinematics modelling for the scalable twisting skeleton of the proposed novel torsional actuator.
- 2) The fabrication process for integrating the foldable twisting skeleton and the square artificial muscle of the torsional actuator.
- 3) A foldable and light-weight torsional actuator capable of large twisting angle under low air pressure.

In the following sections, we first introduce the concept design of torsional actuator augmenting a twisting skeleton and an artificial muscle. Following this process, section III presents the kinematic modelling of the twisting skeleton and the artificial muscle. Section IV details the fabrication process of the twisting skeleton and the artificial muscle. They are then combined together to form a torsional actuator. Section V reports the experimental results of a prototype and section VI gives the conclusion of this paper.

## II. CONCEPT DESIGN OF THE TORSIONAL ACTUATOR

Origami can evolve from 2-dimensional flat sheet model to 3-dimensional complex structure by arranging the sequences of folding creases. The distinct deployability and foldability of origami have wide potential applications in areas such as designing multi-part systems and making soft robots. Here we take the essential principles of origami-folding into consideration and propose a novel torsional actuator.

The 3UU triangle platform and the 4UU square platform in [22], modifications of Wren Platform, are acted as deployable structures for using in uni-dimensional deployment applications. Further, the kinematic analysis of a kinematic variant of Wren platform in [23] reveals that the twisting mechanism consisting of three identical four-link limbs, one

base and one platform in congruent isosceles triangles, can achieve helical motion when it is twisted.

Taking the origami-inspired twisting mechanism as skeleton and incorporating the skeleton with an artificial muscle, a novel torsional actuator is designed and illustrated in Fig. 1. The twisting skeleton consists of a platform, a base and four identical limbs, while the internal structure is composed of a bearing, a bearing connector and an artificial muscle. The role of the internal artificial muscle is to generate force to push and pull the outer skeleton, while the role of outer skeleton is to output torque and achieve the twisting motion.

A square artificial muscle is employed to drive the torsional actuator. This square artificial muscle is made of TPU fabric and constructed by connecting a number of square layers of fabric along their edges. As the thin TPU fabric is extremely soft, the square artificial muscle can be compressed into a configuration of small volume and stored into the base of the twisting skeleton when it is vacuumed. By contrast, it will extend when inflated, thereby achieving a large expansion ratio [24].

## III. KINEMATIC MODELLING OF THE TORSIONAL ACTUATOR

### A. Kinematic model of the twisting skeleton of the torsional actuator

The kinematic model of the twisting skeleton of the torsional actuator is illustrated in Fig. 2. For the sake of better understanding, the base and the platform are represented by two identical crosses denoted by  $\square ABCD$  and  $\square A'B'C'D'$ , respectively.  $A, B, C$  and  $D$  are the common points where the axes of revolute joints  $R_{i1}$  ( $i = 1, 2, 3$  and  $4$ ) and the base are perpendicular and intersected, while  $A', B', C'$  and  $D'$  are the common points where the axes of revolute joints  $R_{i4}$  and the platform are perpendicular and intersected. The point of intersection between lines  $BD$  and  $AC$  on the base is denoted by  $O$ , while the point of intersection between lines  $B'D'$  and  $A'C'$  on the platform is denoted by  $O'$ . The distances from  $O$  to  $A, B, C$  and  $D$  are equal, while the distances from  $O'$  to  $A', B', C'$  and  $D'$  are also the same. Further, axes of the revolute joints  $R_{i1}$  and  $R_{i2}$  in each limb are perpendicular and have common points denoted by  $E, F, G$  and  $H$ , respectively. In comparison, axes of the revolute joints  $R_{i3}$  and  $R_{i4}$  in each limb are perpendicular and have

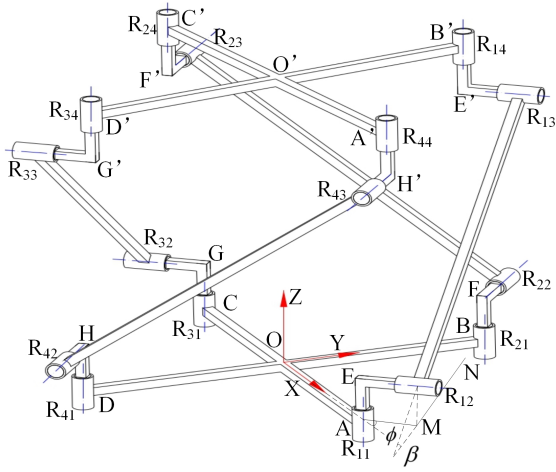


Fig. 2. Kinematic model of the twisting skeleton

common points denoted by  $E'$ ,  $F'$ ,  $G'$  and  $H'$ , respectively. Axes of the revolute joints  $R_{i2}$  and  $R_{i3}$  are parallel and the offsets between any two successive joints in all four limbs are equal.

### B. Helical motion of the twisting skeleton

As shown in Fig. 2, a Cartesian coordinate frame  $O - XYZ$  is set up at the base where the origin of frame is coincident with the midpoint  $O$ ,  $X$  axis passes  $OA$ ,  $Y$  axis passes  $OB$ , and  $Z$  axis follows right hand rule and is collinear with  $OO'$ . Local coordinate frames are also set up for each limb where the origin of each frame is located at  $E$ ,  $F$ ,  $G$  and  $H$ , respectively.  $x_i$  axis is parallel to  $OX$ ,  $y_i$  axis is parallel to  $OY$  and  $z_i$  axis is set through right hand rule. The projection of axis of joint  $R_{12}$  on the base is  $AM$  and the projection of the link connected to joints  $R_{12}$  and  $R_{13}$  is  $MN$ . The angle measured between lines  $OA$  and  $AM$  is defined as  $\phi$ , while the angle measured between line  $MN$  and the link connected  $R_{12}$  and  $R_{13}$  is defined as  $\beta$ . The motion screws of limb 1 composed of joints  $R_{1j}$  ( $j = 1, 2, 3$  and  $4$ ) expressed in the local coordinate frame  $E - x_1y_1z_1$  are

$$\mathbf{S}_1 = \begin{cases} \mathbf{S}_1 = [0 & 0 & 1 & 0 & 0 & 0]^T \\ \mathbf{S}_2 = [c\phi & s\phi & 0 & 0 & 0 & 0]^T \\ \mathbf{S}_3 = [c\phi & s\phi & 0 & -ls\beta s\phi & ls\beta c\phi & -lc\beta]^T \\ \mathbf{S}_4 = [0 & 0 & 1 & lc\beta c\phi & lc\beta s\phi & 0]^T \end{cases} \quad (1)$$

where 'c' and 's' are the abbreviations of  $\cos(*)$  and  $\sin(*)$ , respectively. The reciprocal constraint screws of (1) are derived as

$$\mathbf{S}_1^r = \begin{cases} {}^1\mathbf{S}_{11}^r = [-c\beta s\phi & c\beta c\phi & s\beta & 0 & 0 & 0]^T \\ {}^1\mathbf{S}_{12}^r = [0 & 0 & 0 & -s\phi & c\phi & 0]^T \end{cases} \quad (2)$$

The constraints applied to the platform by limb 1 can be calculated by translating (1) from the local coordinate frame  $E - x_1y_1z_1$  to the global coordinate frame  $O - XYZ$ .

$$\mathbf{S}_{1j}^r = ({}^0\mathbf{T}_1)^{-1} \mathbf{S}_{1j}^r = \begin{bmatrix} \mathbf{I} & \mathbf{0} \\ \mathbf{p} & \mathbf{I} \end{bmatrix} {}^1\mathbf{S}_{1j}^r \quad (3)$$

where

$$\mathbf{p} = \begin{bmatrix} 0 & -b & 0 \\ b & 0 & -a \\ 0 & a & 0 \end{bmatrix}$$

$a$  is the distance of  $OA$  and  $b$  is the distance of  $AE$ .

Since the four limbs of the twisting skeleton are symmetrical, the constraint screws of limbs  $k$  ( $k = 2, 3$  and  $4$ ) can be derived by rotating the screw vector  $\mathbf{S}_1^r$  along  $Z$  axis by  $\alpha = \pi/2, \pi$  and  $3\pi/2$ , respectively.

$$\mathbf{S}_{kj}^r = \begin{bmatrix} \mathbf{R}(\alpha) & \mathbf{0} \\ \mathbf{0} & \mathbf{R}(\alpha) \end{bmatrix} \mathbf{S}_{1j}^r \quad (4)$$

in which

$$\mathbf{R}(\alpha) = \begin{bmatrix} \cos \alpha & -\sin \alpha & 0 \\ \sin \alpha & \cos \alpha & 0 \\ 0 & 0 & 1 \end{bmatrix}$$

The constraint-screw system employed on platform is then derived as

$$\mathbf{S}^r = \begin{cases} \mathbf{S}_{11}^r = [-c\beta s\phi & c\beta c\phi & s\beta & x_{14} & x_{15} & ac\beta c\phi]^T \\ \mathbf{S}_{12}^r = [0 & 0 & 0 & -s\phi & c\phi & 0]^T \\ \mathbf{S}_{21}^r = [-c\beta c\phi & -c\beta s\phi & s\phi & x_{24} & x_{25} & ac\beta c\phi]^T \\ \mathbf{S}_{22}^r = [0 & 0 & 0 & -c\phi & -s\phi & 0]^T \\ \mathbf{S}_{31}^r = [c\beta s\phi & -c\beta c\phi & s\beta & x_{34} & x_{35} & ac\beta c\phi]^T \\ \mathbf{S}_{32}^r = [0 & 0 & 0 & s\phi & -c\phi & 0]^T \\ \mathbf{S}_{41}^r = [c\beta c\phi & c\beta s\phi & s\phi & x_{44} & x_{45} & ac\beta c\phi]^T \\ \mathbf{S}_{42}^r = [0 & 0 & 0 & c\phi & s\phi & 0]^T \end{cases} \quad (5)$$

where

$$\begin{aligned} x_{14} &= -bc\beta c\phi, & x_{15} &= -as\beta - bc\beta s\phi \\ x_{24} &= as\beta + bc\beta s\phi, & x_{25} &= -bc\beta c\phi \\ x_{34} &= bc\beta c\phi, & x_{35} &= as\beta + bc\beta s\phi \\ x_{44} &= -as\beta - bc\beta s\phi, & x_{45} &= bc\beta c\phi \end{aligned}$$

Based on reciprocal screw theory, the motion-screw system of platform is further derived as

$$\mathbf{S}_m = \mathbf{S}_1 = [0 & 0 & 1 & 0 & 0 & -a \cot \beta c\phi]^T \quad (6)$$

It indicates the platform has one degree of freedom (DOF) and can achieve helical motion along  $Z$  axis.

Based on the structure of twisting skeleton, the relationship between twisting angle and height can be derived as

$$\sin \frac{\theta}{2} = \frac{\sqrt{l^2 - h^2}}{2 \cdot r_0} \quad (7)$$

in which  $\theta$  is the twisting angle of the platform corresponding to the base,  $h$  is the distance between the platform and the base,  $l$  is the length of link connecting  $R_{12}$  and  $R_{13}$ , and  $r_0$  is the radius of the circle defined by points  $A, B, C$ , and  $D$ .

### C. Modelling of the square artificial muscle

The function of internal artificial muscle is to drive the twisting skeleton so as to achieve the corresponding motion. A square artificial muscle is designed in this paper since it can achieve a large extension ratio and is lightweight.

The model of square artificial muscle is shown in Fig. 3(a). The force generated by artificial muscle [25] is calculated by

$$F_{\text{drive}} = P \cdot S \quad (8)$$

where  $P$  is the air pressure and  $S$  is the contact area between artificial muscle and bearing connector.

In order to estimate the maximum length of artificial muscle, the chamber which is the unit forming the square artificial muscle can be simplified and modelled as a geometric solid with straight edges [25] (Fig. 3(b)), even though it will have a complex shape in inflated state.  $e$  denotes the length of side where the chamber is bonded to its neighboring chamber,  $f$  is the distance between the edge and the bonded side of the chamber, and  $w$  is the distance across the chamber, which will change when the chamber is being inflated or deflated. The volume of the chamber is calculated by

$$V = \frac{4}{3}w \left( f^2 - \left( \frac{w}{2} \right)^2 \right) + we^2 + 2we \sqrt{f^2 - \left( \frac{w}{2} \right)^2} \quad (9)$$

where the first term is the volume of four corners, the second item is the volume of the central cube, and the last item is the volume of four sides excluding four corners. The configuration of the artificial muscle with maximum volume can be determined by calculating the derivation of  $V$  in (9), i.e. the maximum volume  $V_{\text{max}}$  can be obtained with  $w_{\text{max}}$ .  $w_{\text{max}}$  is used for determining the number of chambers which form an artificial muscle with a design length of  $l_r$ .

$$N = \text{ceil} \left( \frac{l_r}{w_{\text{max}}} \right) \quad (10)$$

## IV. FABRICATION OF THE TORSIONAL ACTUATOR

### A. Additive manufacturing of the twisting skeleton

In order to achieve a large twisting angle of  $90^\circ$ , the design parameters for twisting skeleton should be  $r_0 = l/\sqrt{2}$  based on (7). Here we fabricated a twisting skeleton with  $l = 30\text{mm}$  and  $r_0 = l/\sqrt{2}$ .

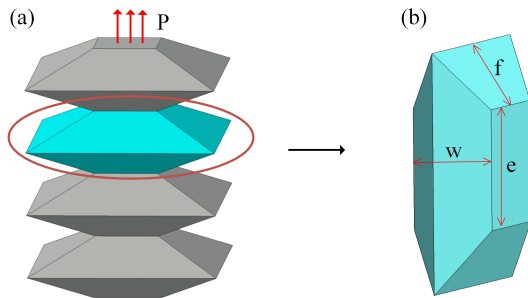


Fig. 3. (a) Model of the square artificial muscle, (b) model of a chamber.

A commercial 3D printer, the Ultimaker 3 with 0.4mm nozzle, was used to print the parts of twisting skeleton, i.e. both the left and right sides of limb illustrated in Fig. 4(a), the platform and the base shown in Fig. 4(c). PLA filament was selected as the printing material.

After printing the parts of twisting skeleton, three-layer structure was employed to design limbs. As shown in Fig. 4(a), the bottom layer is one side of a limb and the top layer is another side of the limb, while TPU membrane with thickness of 0.3 mm is selected as the middle layer to bond other layers together with super glue. As TPU membrane is flexible and resistant to wear and tear, it is used as the joint to connect links.

A limb was obtained (Fig. 4(b)) by bonding three layers shown in Fig. 4(a). This limb was then adhered to the platform and the base (Fig. 4(c)). A twisting skeleton was built though repeating the steps from Fig. 4(a) to Fig. 4(c) to make other three limbs. Fig. 4(d) presents a sample of twisting skeleton.

### B. Fabrication of the artificial muscle

In order insert the artificial muscle into the twisting skeleton, the design parameters of artificial muscle are  $f = 8\text{mm}$ ,  $e = 8\text{mm}$  and  $l_r = 30\text{mm}$ . When  $w_{\text{max}} = 11.69\text{mm}$ , the maximum volume is  $V = 2234.68\text{mm}^3$  calculated by (9). The number of chambers for making artificial muscle is

$$N = \text{ceil} \left( \frac{l_r}{w_{\text{max}}} \right) = \text{ceil} \left( \frac{30}{11.69} \right) = 3 \quad (11)$$

Considering both mechanical properties and compatibility with other materials, air tight TPU membrane was chosen to fabricate the artificial muscle. The crystallisation temperature of TPU membrane is  $156^\circ\text{C}$  and the melting point is  $260^\circ\text{C}$  [26], so the heating temperature can be set in the range of  $[156, 260]^\circ\text{C}$  for laminating TPU membranes to form a chamber.

In order to laminate TPU membranes together, a PTFE slice with a square hole (Fig. 4(e)) was employed as the middle layer. Since PTFE has a low coefficient of friction and is non-stick with most materials even in high temperature, it can prevent the adhesion of two TPU membranes excluding the area of square hole.

After aligning there layers (Fig. 4(e)), a heat press machine with heating temperature at  $160^\circ\text{C}$  was applied to press layers. Then a chamber was obtained (Fig. 4(f)) by removing the PTFE slide.

A hole was made in in the chamber for the purpose of pressure air supply. A sample of the chamber is shown in Fig.4 (g). Heat sealer was then used to connect chambers by sealing four edges of each chamber with its neighboring chamber. Fig. 4(h) presents continuous three chambers based on the calculation in (10).

In order to fabricate an air inlet, a small hole was made in a TPU membrane. Then a silicone tubing with 4 mm outer diameter (OD) was inserted into the hole. Other two tubes with 4 mm inner diameter and 6 mm outer diameter, one inserted from the end of thinner tubing and another inserted

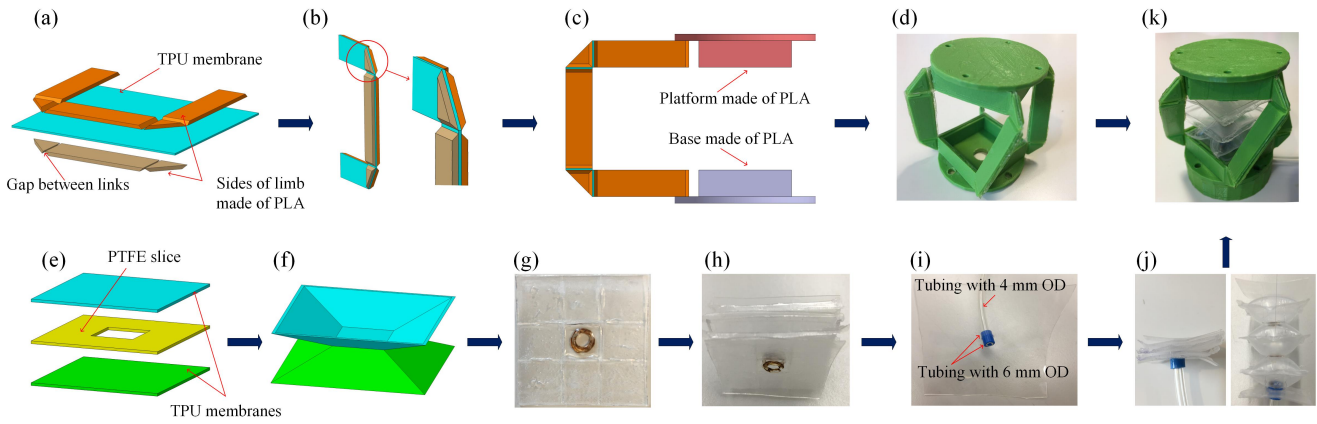


Fig. 4. Steps of fabrication of torsional actuator augmenting a twisting skeleton and an artificial muscle. (a) lamination with PLA 3D printed parts and TPU membrane, (b) a limb of twisting skeleton, (c) limb bonded with platform and base, (d) a sample of twisting skeleton, (e) lamination with TPU membranes and PTFE slice, (f) a chamber of artificial muscle, (g) a sample of the chamber with a central hole, (h) continuous chambers, (i) fabrication of air inlet, (j) artificial muscle under vacuum and inflation, (k) a prototype of torsional actuator.

from the other end of thinner tubing, were lying outside of the thinner tubing. Then thicker tubes firmly covered the hole by pushing and bonding both together, as shown in Fig. 4(i).

The square artificial muscle was completed by sealing the continuous chambers and the TPU membrane with an air inlet. Fig. 4(j) demonstrates an artificial muscle under vacuum and inflation, respectively. Then a bearing and a bearing connector were utilized to connect the artificial muscle with the twisting skeleton. A prototype of torsional actuator is presented in Fig. 4(k).

## V. EXPERIMENTS OF THE TORSIONAL ACTUATOR

In order to test the performance of the torsional actuator, a pneumatic control system (Fig. 5) is built. A pneumatic regulator, SMC ITV-212BL4, is used to control the air pressure. The inlet of pneumatic regulator is connected with air compressor, while the outlet is connected to the torsional actuator and supplies pressure air. The output pressure of the pneumatic regulator is controlled by voltage signals programmed through the controller Arduino using its accessory software. Linear-torsion testing machine, Instron E10000, is

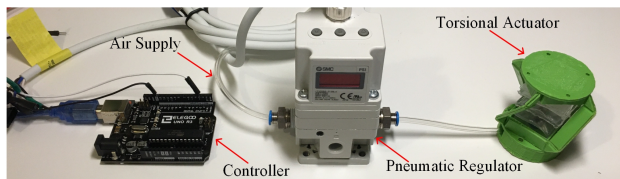


Fig. 5. Pneumatic control system for the test of torsional actuator

utilized to control the position of the prototype and also record the parameters including torque, force, displacement and rotation angle, as shown in Fig. 7(a). (A video in the supplementary information is attached for the tests.)

In order to verify the helical motion of torsional actuator, the twisting angle and height at different positions were measured, as shown in Fig. 6(a). The red dots in Fig. 6(b) are plotted from experimental data, while the black curve is

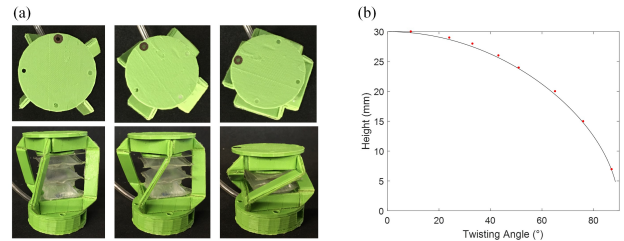


Fig. 6. Helical motion verification. (a) measurements of twisting angle and height, (b) relation between twisting angle and height.

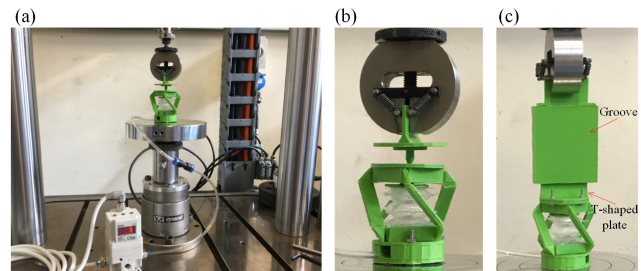


Fig. 7. (a) Linear-torsion testing machine, (b) test of driving force, (c) test of output torque.

drawn from (7). It is clear that these experimental data are very close to the theoretical curve, so the derivation in (7) is right and torsional actuator is able to achieve helical motion.

The role of artificial muscle is to drive the twisting skeleton, so the driving force generated by artificial muscle should be tested. The testing machine is utilized to test the driving force by fixing the torsional actuator at different heights and varying the air pressure from 1Psi to 8Psi, as illustrated in Fig. 7(b). The driving force is measured using the transducer in Instron E10000, while the air pressure is showed on the screen of pneumatic regulator.

The results in Fig. 8(a) show that the driving force is proportional to the air pressure at a given height of the torsional actuator. The proportionality coefficient between

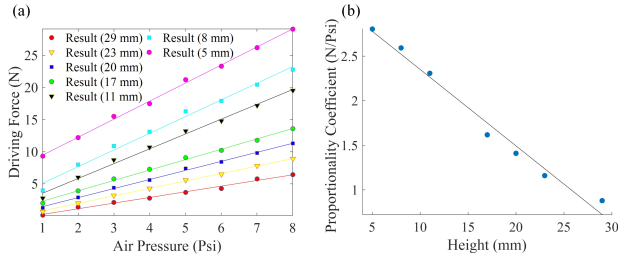


Fig. 8. (a) Driving force at air pressures, (b) PCFP at different heights.

driving force and air pressure (PCFP) increases with the decline of height. Fig. 8(b) illustrates the relationship between PCFP and height is approximate to linearity. Therefore, the fitting straight line in Fig. 8(b) can be used to determine the PCFP of the torsional actuator at different heights, thereby calculating the driving force of the torsional actuator.

The proportional relationship between driving force and air pressure at a given height matches the model in (8). However, the PCFP varies at different heights due to the change in contact area between artificial muscle and bearing connector. The diameter of the bearing connector is  $28\text{mm}$ , while the bonded area between artificial muscle and bearing connector is  $10\text{mm} \times 10\text{mm}$ . This connection can be seen in Fig. 1(a). When the artificial muscle is fully inflated, the contact area is approximate to the bonded area. By contrast, when the height of torsional actuator decreases, the artificial muscle is compressed, which increases the contact area, thereby increasing the driving force and PCFP.

The role of twisting skeleton is to convert driving force into output torque, so the relation between driving force and output torque also should be tested. A connector incorporating a groove and a T-shaped plate (Fig. 7(c)) is made to transmit torque and allow translational movement.

By fixing the twisting angle of the gripper of Instron E10000 and varying the air pressure from  $1\text{Psi}$  to  $8\text{Psi}$ , the output torque and air pressure are measured. The air pressure is then mapped to the driving force based on the results in Fig. 8. The experimental results in Fig. 9(a) illustrate that the output torque is proportional to the driving force at a giving twisting angle. Further, as twisting angle increases (Fig.9(b)), the variation of the proportionality coefficient between output torque and driving force (PCTF) is approximate to a parabola. The trend of this parabola significantly increases until  $55^\circ$  and then gradually goes up to  $90^\circ$ , which is the upper limit of rotation of the torsional actuator.

The proposed torsional actuator is aim to achieve rotation and generate output torque, so the relationship among twisting angle, air pressure and output torque are drawn in Fig. 10 based to the above experimental data. Fig. 10(a) shows that the torsional actuator is able to achieve large twisting angle and generate output torque, whereas Fig. 10(b) illustrates that the output torque is proportional to the air pressure at a certain twisting angle.

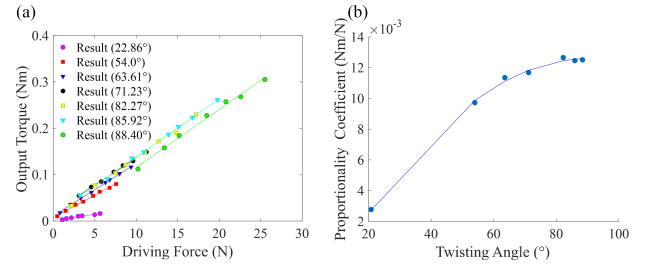


Fig. 9. (a) Relation between driving force and output torque, (b) PCTF at different twisting angles.

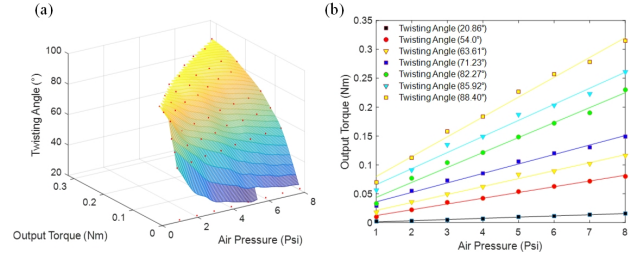


Fig. 10. (a) Relationship among twisting angle, air pressure and output torque, (b) output torque at different air pressures.

## VI. CONCLUSIONS

This paper presents the design and fabrication approach of a novel torsional actuator augmenting an origami-inspired twisting skeleton and a square artificial muscle. The kinematic modelling of the twisting skeleton indicates it has one DOF and is capable of helical motion. A square artificial muscle is designed to drive the twisting skeleton. Based on the proposed fabrication approaches, a prototype of torsional actuator is produced and its performance is tested. Experimental results show that for a given height or twisting angle, the relationship between air pressure, driving force and output torque is proportional. Further, when the height decreases or the twisting angle increases, the driving force and output torque generated by torsional actuator will increase at a given air pressure. The proposed torsional actuator is capable achieve a large twisting angle under low air pressure.

The proposed design and fabrication approaches of torsional actuator are beneficial to scalability of size and forces, and has promising potential for the applications in extreme environments like radiation. The combination of technologies including 3D printing and thermal lamination also provides a cost effective approach for fabricating torsional actuator to actuate robotic devices.

Future work will focus on the position control and force control of novel robotic systems driven by the proposed torsional actuator and deployment in extreme conditions such as nuclear plants, flammable gas and oil environments.

## ACKNOWLEDGMENT

The authors thank Dr Erica Di Federico, who helped in testing the torsional actuator presented in this paper.

## REFERENCES

- [1] M. Hutter, C. Gehring, M. Bloesch, M. A. Hoepflinger, C. D. Remy, and R. Siegwart, "StarlETH: A compliant quadrupedal robot for fast, efficient, and versatile locomotion," *Adaptive Mobile Robotics*, pp. 483-490, 2012.
- [2] C. Semini, N. G. Tsagarakis, E. Guglielmino, M. Focchi, F. Cannella, and D. G. Caldwell, "Design of HyQ—a hydraulically and electrically actuated quadruped robot," *Proceedings of the Institution of Mechanical Engineers, Part I: Journal of Systems and Control Engineering*, vol. 225, no. 6, pp. 831-849, 2011.
- [3] S. Seok, A. Wang, D. Otten, and S. Kim, "Actuator design for high force proprioceptive control in fast legged locomotion," in *2012 IEEE/RSJ International Conference on Intelligent Robots and Systems, IEEE*, pp. 1970-1975, 2012.
- [4] J. Lee, J. Hwangbo, L. Wellhausen, V. Koltun, and M. Hutter, "Learning quadrupedal locomotion over challenging terrain," *Science Robotics*, vol. 5, no. 47, 2020.
- [5] Z. Jiao, C. Ji, J. Zou, H. Yang, and M. Pan, "Vacuum-Powered Soft Pneumatic Twisting Actuators to Empower New Capabilities for Soft Robots," *Advanced Materials Technologies*, vol. 4, no. 1, p. 1800429, 2019.
- [6] Z. Jiao, C. Zhang, W. Wang, M. Pan, H. Yang, and J. Zou, "Advanced Artificial Muscle for Flexible Material-Based Reconfigurable Soft Robots," *Advanced Science*, vol. 6, no. 21, p. 1901371, 2019.
- [7] S. T. Mahon, A. Buchoux, M. E. Sayed, L. Teng, and A. A. Stokes, "Soft robots for extreme environments: Removing electronic control," in *2019 2nd IEEE International Conference on Soft Robotics (RoboSoft)*, IEEE, pp. 782-787, 2019.
- [8] D. Rus and M. T. Tolley, "Design, fabrication and control of soft robots," *Nature*, vol. 521, no. 7553, pp. 467-475, 2015.
- [9] K. Zhang and K. Althoefer, "Designing origami-adapted deployable modules for soft continuum arms," in *Annual Conference Towards Autonomous Robotic Systems*, Springer, pp. 138-147, 2019.
- [10] S. Aziz and G. M. Spinks, "Torsional artificial muscles," *Materials Horizons*, vol. 7, no. 3, pp. 667-693, 2020.
- [11] B. Tondu, K. Braikia, M. Chettouh, and S. Ippolito, "Second order sliding mode control for an anthropomorphic robot-arm driven with pneumatic artificial muscles," in *2009 9th IEEE-RAS International Conference on Humanoid Robots, IEEE*, pp. 47-54, 2009.
- [12] B. Tondu, "Modelling of the McKibben artificial muscle: A review," *Journal of Intelligent Material Systems and Structures*, vol. 23, no. 3, pp. 225-253, 2012.
- [13] S. Sanan, P. S. Lynn, and S. T. Griffith, "Pneumatic torsional actuators for inflatable robots," *Journal of Mechanisms and Robotics*, vol. 6, no. 3, 2014.
- [14] T. Tachi, "Rigid-foldable thick origami," *Origami*, vol. 5, pp. 253-264, 2011.
- [15] E. T. Filipov, T. Tachi, and G. H. Paulino, "Origami tubes assembled into stiff, yet reconfigurable structures and metamaterials," *Proceedings of the National Academy of Sciences*, vol. 112, no. 40, pp. 12321-12326, 2015.
- [16] D. Jeong and K. Lee, "Design and analysis of an origami-based three-finger manipulator," *Robotica*, vol. 36, no. 2, pp. 261-274, 2018.
- [17] A. Pagano, T. Yan, B. Chien, A. Wissa, and S. Tawfick, "A crawling robot driven by multi-stable origami," *Smart Materials and Structures*, vol. 26, no. 9, p. 094007, 2017.
- [18] S.-J. Kim, D.-Y. Lee, G.-P. Jung, and K.-J. Cho, "An origami-inspired, self-locking robotic arm that can be folded flat," *Science Robotics*, vol. 3, no. 16, 2018.
- [19] S. Felton, M. Tolley, E. Demaine, D. Rus, and R. Wood, "A method for building self-folding machines," *Science*, vol. 345, no. 6197, pp. 644-646, 2014.
- [20] S. Li, D. M. Vogt, D. Rus, and R. J. Wood, "Fluid-driven origami-inspired artificial muscles," *Proceedings of the National Academy of Sciences*, vol. 114, no. 50, pp. 13132-13137, 2017.
- [21] M. Salerno, K. Zhang, A. Menciassi, and J. S. Dai, "A novel 4-DOF origami grasper with an SMA-actuation system for minimally invasive surgery," *IEEE Transactions on Robotics*, vol. 32, no. 3, pp. 484-498, 2016.
- [22] G. Kiper and E. Söylemez, "Modified Wren platforms," in *13th IFToMM world congress, Guanajuato, Mexico*, vol. 814, 2011.
- [23] K. Zhang and J. Dai, "Reconfiguration analysis of wren platform and its kinematic variants based on reciprocal screw systems," in *Proceedings of the 14th IFToMM World Congress*, pp. 237-242, 2015.
- [24] T. Ranzani, S. Russo, F. Schwab, C. J. Walsh, and R. J. Wood, "Deployable stabilization mechanisms for endoscopic procedures," in *2017 IEEE International Conference on Robotics and Automation (ICRA)*, IEEE, pp. 1125-1131, 2017.
- [25] H. D. Yang, B. T. Greczek, and A. T. Asbeck, "Modeling and analysis of a high-displacement pneumatic artificial muscle with integrated sensing," *Frontiers in Robotics and AI*, vol. 5, p. 136, 2019.
- [26] K. Zhang, Y. Zhu, C. Lou, P. Zheng, and M. Kovač, "A design and fabrication approach for pneumatic soft robotic arms using 3D printed origami skeletons," in *2019 2nd IEEE International Conference on Soft Robotics (RoboSoft)*, IEEE, pp. 821-827, 2019.